engineering proceedings

MDPI

Proceeding Paper

Analysis of GNSS Time Series Recorded on South Shetland Island and Antarctic Peninsula during the Geodynamic Activity in 2020 of the Orca Underwater Volcano (Brandfield Sea Rift, Antarctica) †

Belén Rosado [1,*], Alejandro Pérez-Peña [1], Paola Barba [1], Javier Ramírez-Zelaya [1], Enrique Carmona [2], Rosa Martín [2], Vanessa Jiménez [2], Jorge Gárate [1], Amós de Gil [1] and Manuel Berrocoso [1]

[1] Laboratorio de Astronomía, Geodesia y Cartografía, Departamento de Matemáticas, Facultad de Ciencias, Campus de Puerto Real, Universidad de Cádiz, 11510 Puerto Real, Spain; alejandro.perezpena@uca.es (A.P.-P.); paola.barba@uca.es (P.B.); javierantonio.ramirez@uca.es (J.R.-Z.); jorge.garate@uca.es (J.G.); amos.degil@uca.es (A.d.G.); manuel.berrocoso@uca.es (M.B.)

[2] Instituto Andaluz de Geofísica, Universidad de Granada, 18071 Granada, Spain; ecarmona@ugr.es (E.C.); rosa@ugr.es (R.M.); vanessa.jimenez@uca.es (V.J.)

* Correspondence: belen.rosado@uca.es

† Presented at the 9th International Conference on Time Series and Forecasting, Gran Canaria, Spain, 12–14 July 2023.

Abstract: The region defined by the South Shetland Islands, Bransfield Sea, and Antarctic Peninsula has complex geodynamic activity resulting from the active subduction process of the Phoenix Plate under the Antarctic Plate. This subduction produces a rift of expansion along the Bransfield Sea basin between the South Shetland Islands and the Antarctic Peninsula. There is also a chain of submarine (Orca, Three Sisters, and Building A) and emerged (Deception and Pinguin) volcanoes. In 2020, there was intense seismic activity around the Orca volcano with earthquakes of up to 6.9 Mw. This paper presents displacement models of this seismic activity produced in the region. The geodetic time series of the GNSS stations located in the region were analyzed: UYBA at the Uruguayan Artigas Antarctic Base (King George Island) and PAL2 at the U.S. Palmer Antarctic Base (Anvers Island). These data were taken from the Nevada Geodetic Laboratory.

Keywords: GNSS system; geodetic time series; geodynamic; volcano–tectonic deformation

Citation: Rosado, B.; Pérez-Peña, A.; Barba, P.; Ramírez-Zelaya, J.; Carmona, E.; Martín, R.; Jiménez, V.; Gárate, J.; de Gil, A.; Berrocoso, M. Analysis of GNSS Time Series Recorded on South Shetland Island and Antarctic Peninsula during the Geodynamic Activity in 2020 of the Orca Underwater Volcano (Brandfield Sea Rift, Antarctica). *Eng. Proc.* **2023**, *39*, 25. https://doi.org/10.3390/engproc2023039025

Academic Editors: Ignacio Rojas, Hector Pomares, Luis Javier Herrera, Fernando Rojas and Olga Valenzuela

Published: 29 June 2023

1. Introduction

Due to innovations and exponential advances over the past three decades, GNSS–GPS systems have become important tools in geodesy and geophysics, pushing forward the science and precise measurement of the Earth's various active processes on land, water, and ice, and in the atmosphere. Nowadays, GPS systems are essential components of the newest generation of Earth science and natural hazard assessment capabilities for monitoring and understanding earthquakes, volcanoes, and tsunamis, among others.

From the processing of the GPS observations, geodetic time series with subcentrimetric accuracy are obtained. GPS geodetic time-series analysis allows the study of the geodynamic behavior of a specific terrestrial area. These time series define the temporal evolution of the geocentric or topocentric coordinates obtained from geodetic stations, which are linear or nonlinear depending on the tectonic or volcanic–tectonic characteristics, respectively, of a region. Linear series are easily modeled, but for the study of nonlinear series, it is necessary to apply filtering techniques that provide a more detailed analysis of their behavior.

This work focused on the analysis of the geodynamic activity that occurred in 2020 in the region between the South Shetland Islands and the Antarctic Peninsula, close to the

ORCA volcano. For this, the time series of the stations located in the region were analyzed. These stations were UYBA at the Uruguayan Artigas Antarctic Base (King George Island) and PAL2 at the U.S. Palmer Antarctic Base (Anvers Island). For a better understanding of the geodynamic process, the preseismic, coseismic, and postseismic velocities were obtained. The analysis was extended by adding geodesic stations located in the region. All time series were provided by the Nevada Geodetic Laboratory (NGL).

2. Geodynamic Frame

The South Shetland Islands, the Bransfield Sea, and the Antarctic Peninsula define a geodynamically highly complex region. Two major tectonic plates converging in this region: the South American and Antarctic Plates. The boundary between both plates is even more complex due to the interaction of four minor tectonic plates: the Scotia, South Sandwich, Phoenix, and South Shetland plates; and two fracture zones, Shackethlon and Hero Figure 1 [1].

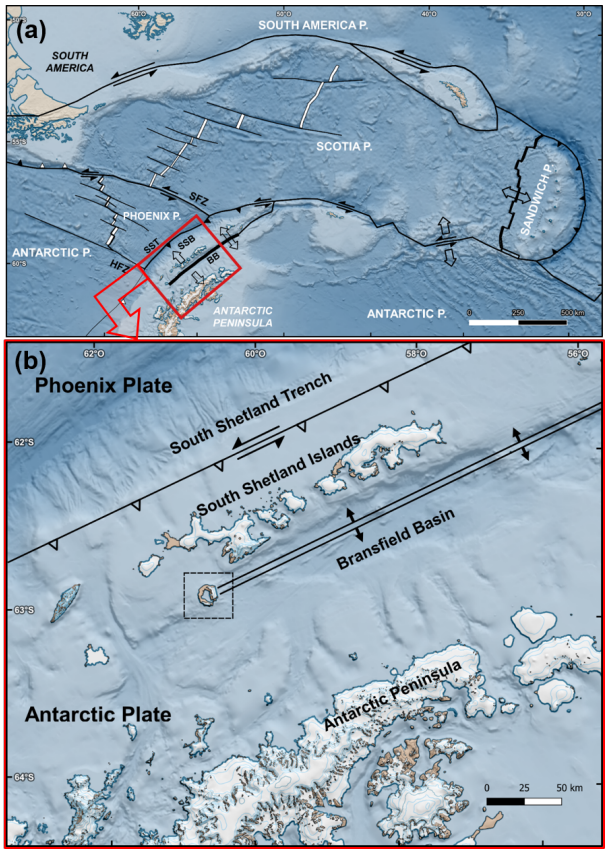

Figure 1. (**a**) Map of the Scotia microplate area and the most important plates boundaries. SST = South Shetland Trench; SSB = South Shetland Block; SFZ = Shackleton Fracture Zone; BB = Bransfield Basin; SOM = South Orkney Microcontinent. (**b**) Map of the Bransfield Strait and the South Shetland Islands showing the main faults in the region.

This region is a seismically active area, where more than 200 earthquakes of magnitude greater than 4 have occurred in the last 50 years (ISC catalogue). Most of these events have been shallow (<10 km) and, in some cases, have taken place at intermediate depths, which indicates the presence of active subduction of the Drake plate under the South Shetland continental block [2]. Seismic activity in the Bransfield Strait usually appears in the form of seismic swarms [3], which are usually located in the vicinity of volcanic edifices.

The largest recent series in Bransfield Strait took place in the Orca volcano area from from August 2020 to November 2021. The Orca volcano is a seafloor caldera shield volcano with a 900 m bathymetric height offshore the coast of King George Island. The epicentral

locations (Figure 2) cluster in the region NE of the Orca volcano (USGS catalogue). The series has originated more than 80,000 earthquakes between King George Island and the Orca submarine volcano with maximum depths of up to approx. 10 km [4]. It started on 28 August 2020 and lasted approximately one year (September 2021). The greatest number of events in the series occurred in the first few months [5]. During this swarm, two cumulative seismic moments in the Bransfield Strait occurred: the first one in November 2020, when the greatest number of events with M > 4 occurred, along with the first largest earthquake (5.9 Mw) located near the Orca volcano; the second one in January 2021, with the biggest earthquake of the swarm (6.9 Mw), located more easterly, outside the Orca region (Figure 3). Most of moment tensor solutions were strike-slip and normal faults with a predominantly NWSE T-axis azimuth (GCMT catalogue, [4]).

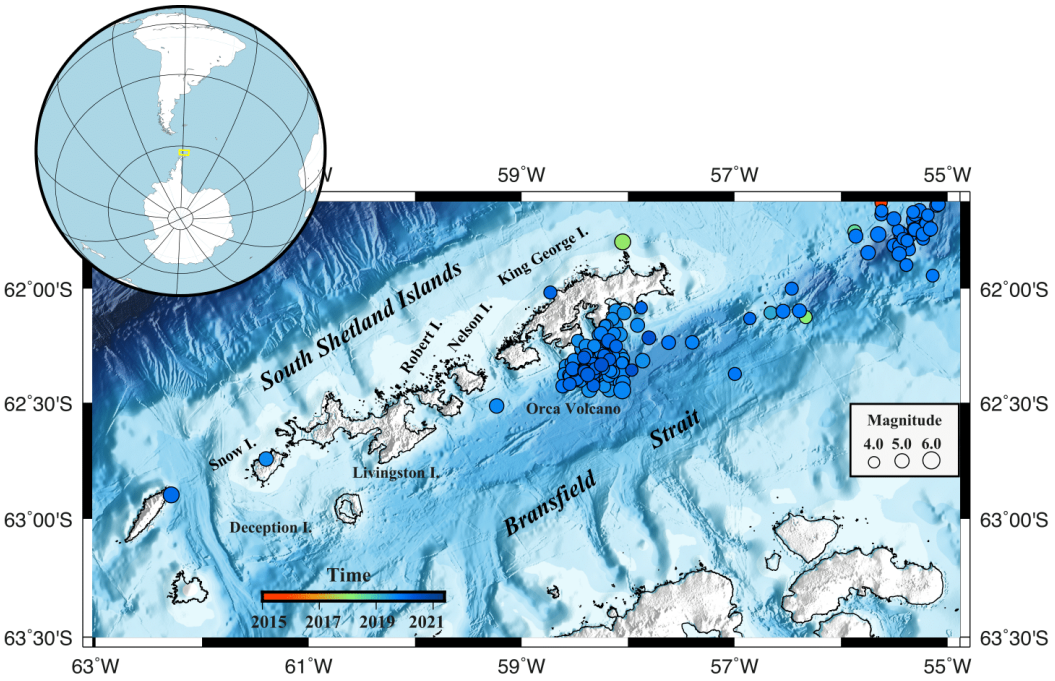

Figure 2. Epicentral map of seismic activity in the South Shetland Islands in the period 2015–2022 for earthquakes with magnitude greater than 4.0 (USGS catalogue).

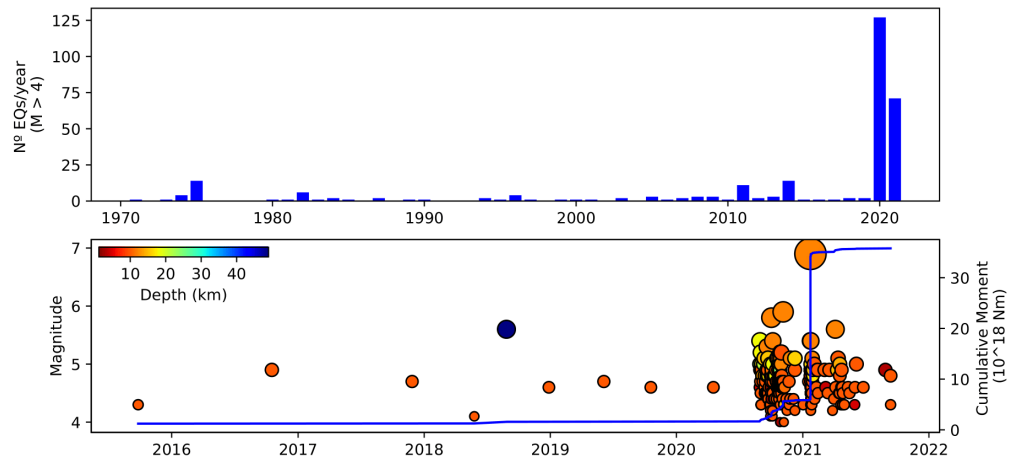

Figure 3. Histogram of number of events per year since 1971 (**top**). Histogram of number of events since 2015 by year, magnitude, and depth; plot of cumulative moment (**below**).

3. Data and Methods

3.1. Geodetic Stations and Data Processing

The time series analyzed in this study were from the geodetic stations provided by the Nevada Geodetic Laboratory (NGL). NGL collects and processes geodetic-quality GPS observations at more than 17,000 stations worldwide from many regional and commercial networks in addition to the commonly used International GNSS Service (IGS) network [6], (Figure 4). The system produces and makes publicly available data products such as position coordinates (latitude, longitude, and height) for geodetic-quality GPS stations around the globe with various data intervals and reference frames that might be useful to users [7]. NGL routinely processes the observations by using GipsyX version 1.0 software [8], released by the Jet Propulsion Laboratory (JPL), which has precise point positioning [9]. JPL's Repro3 final GPS orbits and clocks are also used. More details on the data-processing strategy are given in http://geodesy.unr.edu/gps/ngl.acn.txt. Data accessed on 1 June 2023.

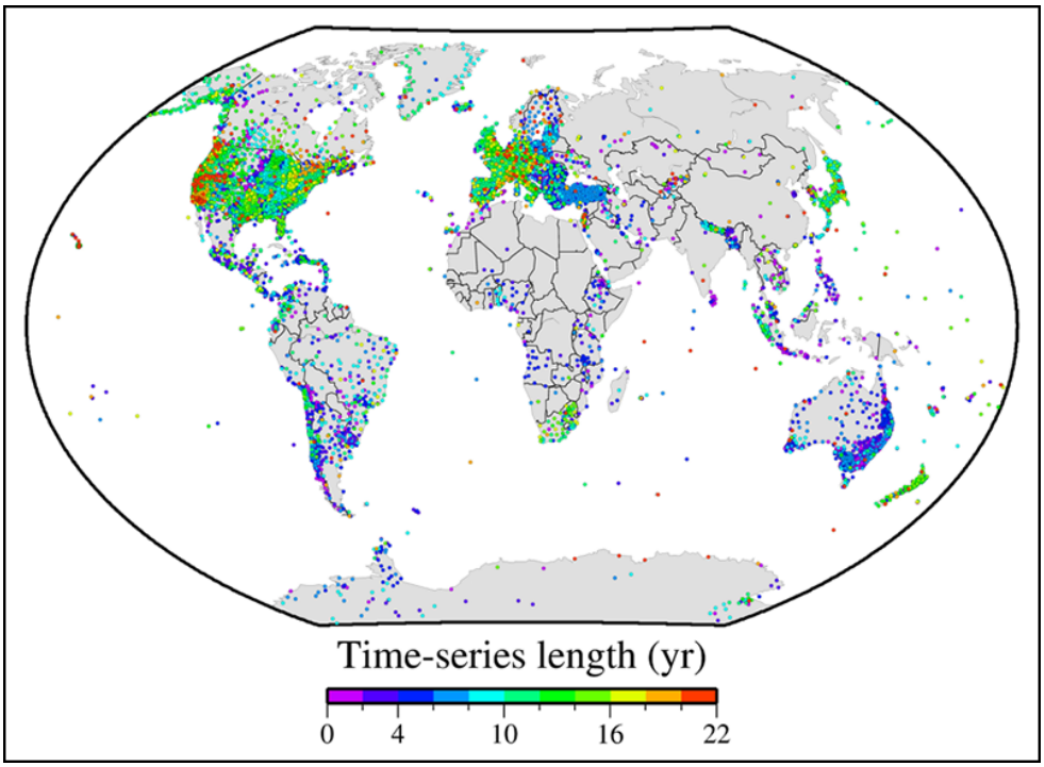

Figure 4. Geodetic GPS stations processed by the Nevada Geodetic Laboratory. Figure taken from [7].

NGL also routinely updates station velocities in the global reference frame, which can be used to capture the rates of deformation of the Earth's surface [7]. These velocities are robustly estimated using the Median Interannual Difference Adjusted for Skewness (MIDAS). This technique is explained in the next section.

3.2. Methodology

The methodology is summarized in Figure 5. First, the topocentric time series of the UYBA and PAL2 stations were obtain from NGL. A descriptive analysis of these time series was carried out, adding the seismic events that occurred from 2015 to 2023. Thus, an initial visualization of the data was carried out, correlating the jumps in the series with the seismic events.

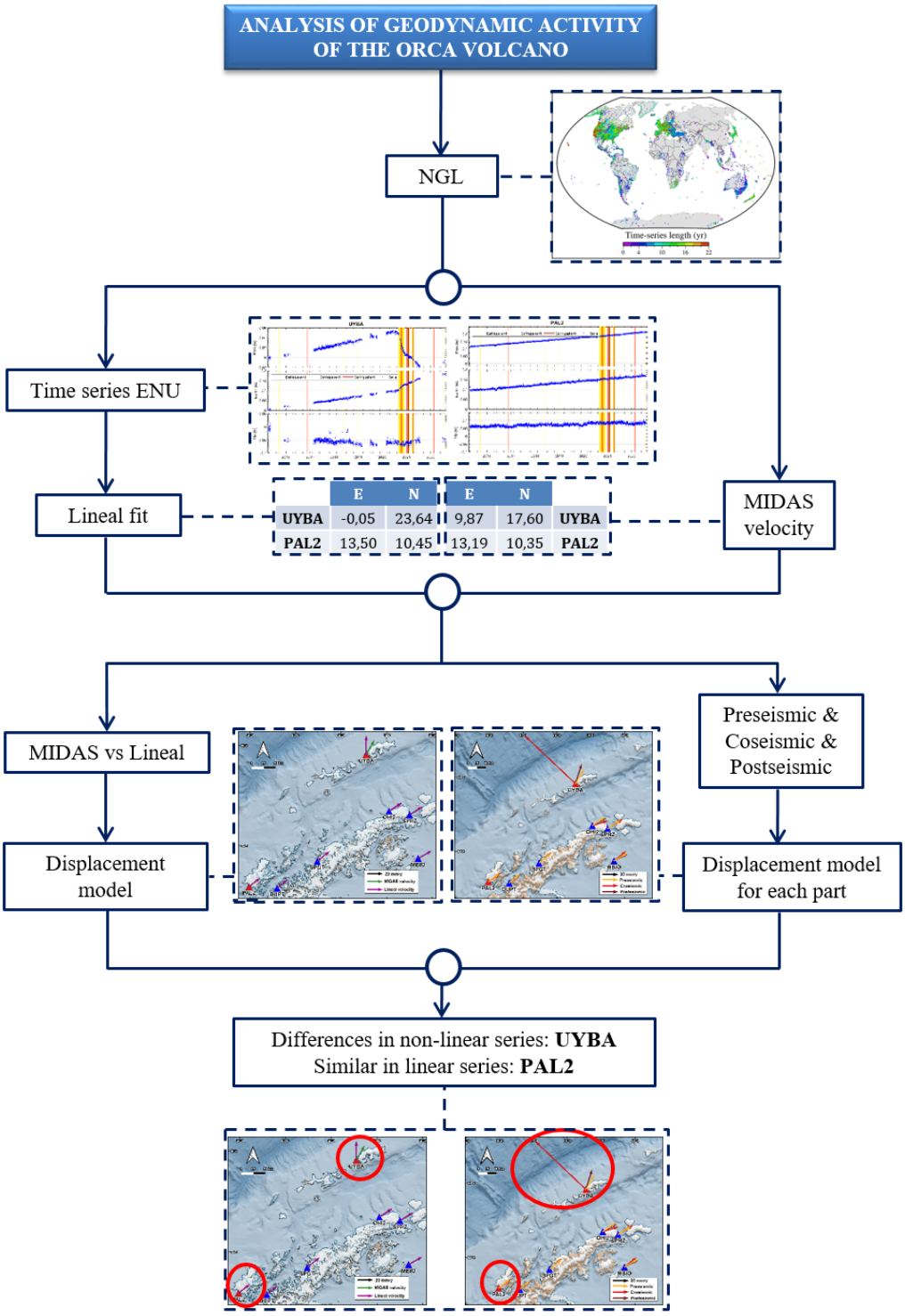

Figure 5. Scheme of the methodology.

Linear series are easily modeled, but for the study of nonlinear series, it is necessary to apply techniques that provide a more detailed analysis of their behavior [10,11]. For this reason, to estimate the trend in the series, two techniques were applied: a linear fit and the MIDAS technique. The trend obtained from the linear fit was valid if the series presented a linear behavior (PAL2 time series). For nonlinear series (UYBA time series), the MIDAS estimator was applied.

MIDAS is a median-based GPS station velocity estimator that is insensitive to outliers, seasonality, step functions (abrupt changes) arising from earthquakes or equipment changes, and statistical data variability [12]. MIDAS also provides velocity error bars based on subsampling the data that prove to be realistic, for example, when comparing the estimated velocities of stations that are close to each other or are separated by a tectonically stable region. MIDAS rates were estimated for all stations with at least one year of data and sufficiently dense time series. In cases where a large earthquake (Mw > 6.9) had occurred near enough to the station, an exponential decay function was solved: $A(1 - e^{-(t-t_0)/\tau})H(t - t_0)$, where t_0 is the time of the earthquake, τ is a relaxation time, A is the amplitude of the decay, and H is the Heaviside step function. In these cases, the background trends were solved after the exponential terms have been removed to obtain a self-consistent model for the time series [12].

Subsequently, displacement models of the region were obtained for each estimated velocity. On the other hand, the velocity of the preseismic, coseismic, and postseismic phases were estimated; the corresponding displacement models were obtained. The idea of the seismic cycle was developed by Harry Fielding Reid to explain his observations of the San Francisco earthquake of 1906. The earthquake-related deformation cycle consists mainly of four phases (Figure 6): the preseismic (nucleation), interseismic (long periods between large earthquakes during which elastic strain accumulation occurs in the broad region), coseismic (brief period during which the accumulated strain is released during earthquakes), and postseismic (the period immediately after an earthquake) phases, which exhibits relatively higher rates of deformation wherein the material deforms in response to the sudden coseismic release of strain [13].

Following this methodology, differences were detected between the behavior of linear and nonlinear time series.

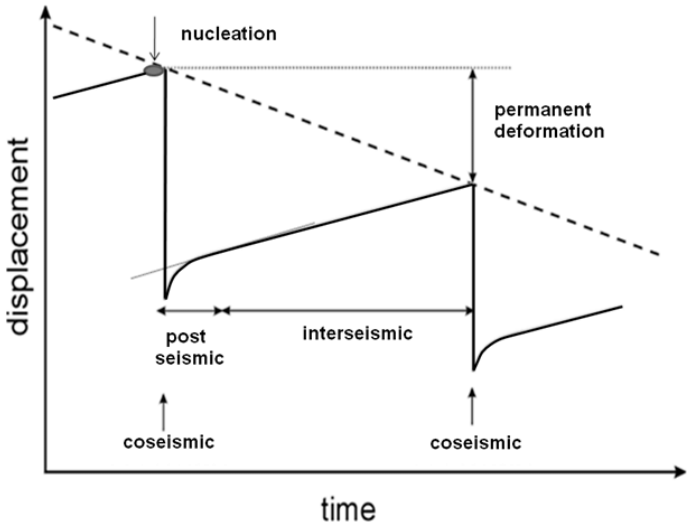

Figure 6. An idealized seismic cycle constituting four distinct phases: preseismic, interseismic, coseismic, and postseismic phases. Figure taken from [13].

4. Results

4.1. Time Series of the UYBA and PAL2 Stations

Figure 7 shows the topocentric time series of the UYBA (Figure 7a) and PAL2 (Figure 7b) stations from 2015 to 2023, represented in blue. These figures also include the seismic events that occurred in that period: earthquakes of magnitude between four and five in yellow, between five and six in orange, and earthquakes greater than six in red.

The PAL2 station is located at the U.S. Palmer Antarctic Base, on Anvers Island. These series are not affected by the geodynamic activity of the ORCA volcano. Therefore, its time series present a linear behavior in all components. The UYBA station is located at

the Uruguayan Artigas Antarctic Base, on King George Island. This station is affected by the geodynamic process that occurred in 2020 at the ORCA volcano, so its time series are nonlinear.

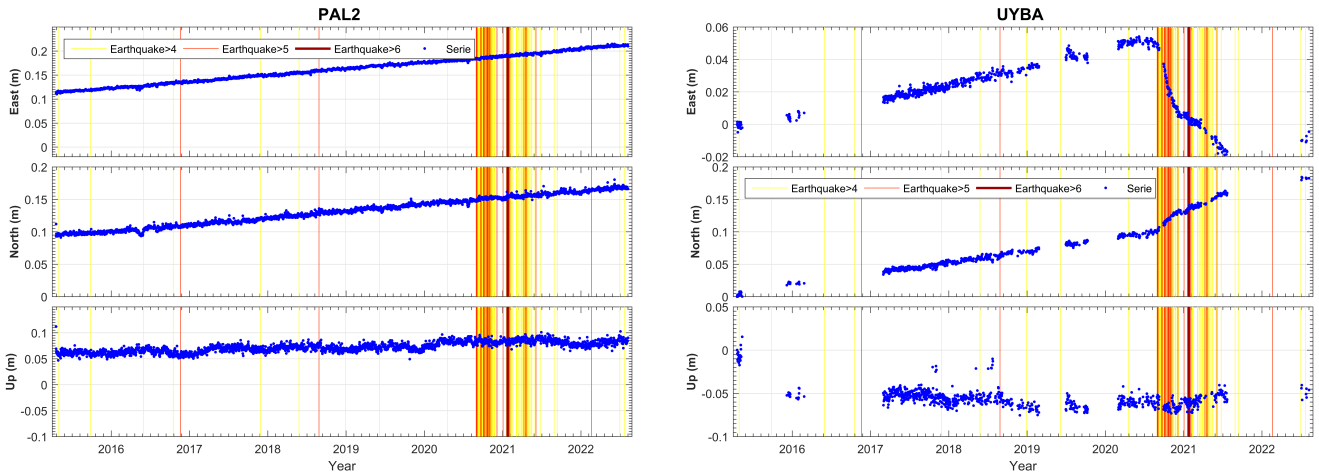

(**a**) (**b**)

Figure 7. Topocentric time series analyzed in this study. Seismic events were included: earthquakes of magnitude between 4 and 5 in yellow, between 5 and 6 in orange, and earthquakes greater than 6 in red. (**a**) Topocentric time series from PAL2 GNSS station located at the U.S. Palmer Antarctic Base, on Anvers Island. (**b**) Topocentric time series from UYBA GNSS station located at the Uruguayan Artigas Antarctic Base, on King George Island.

4.2. Evaluation of MIDAS Velocities versus Linear Velocities

Table 1 shows the velocities obtained from the linear fit and from the MIDAS estimator. For a better understanding, displacement models of the region were obtained for each estimated velocity (Figure 8).

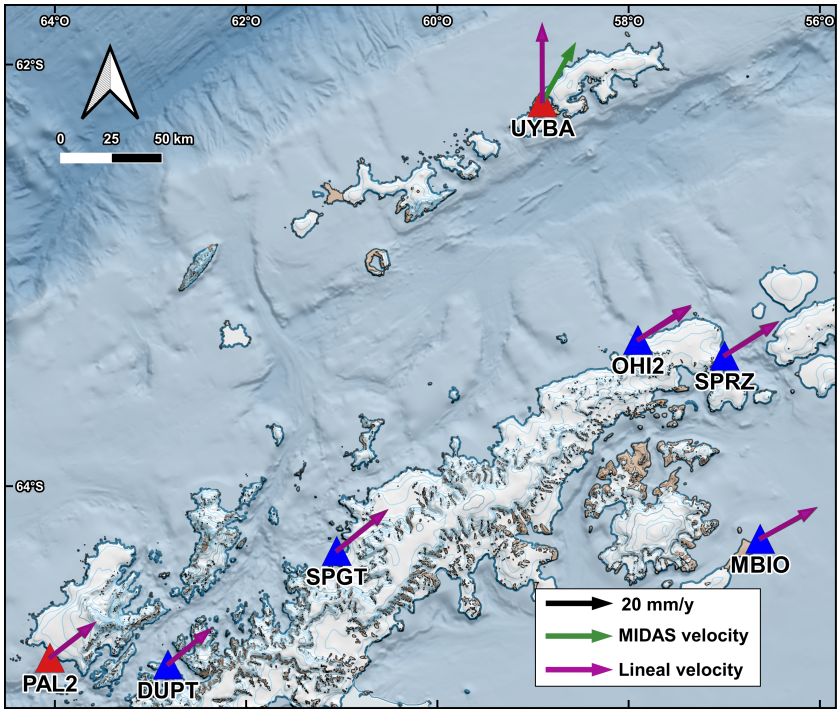

Figure 8. Displacement model of the region.

Table 1. Comparison of MIDAS velocities vs. linear fit, in mm/year.

	UYBA		PAL2	
Velocitt	**East**	**North**	**East**	**North**
MIDAS	9.87	17.60	13.19	10.35
Linear	−0.05	23.64	13.50	10.45

4.3. Preseismic, Coseismic, and Postseismic Displacement Models

The preseismic, coseismic, and postseismic phases were calculated for each component of the time series. The velocities of each phase are shown in Table 2. The different phases considered are shown in Figure 9, together with the velocity in millimeters per year (inset). The corresponding displacement model of each phase is shown in Figure 10.

Table 2. The preseismic, coseismic, and postseismic velocities in mm/year for UYBA and PAL2 stations.

	UYBA		PAL2	
Velocity	**East**	**North**	**East**	**North**
Preseismic	10.62	17.82	13.37	10.48
Coseismic	−64.78	61.38	13.92	9.55
Postseismic	7.79	24.70	14.94	11.09

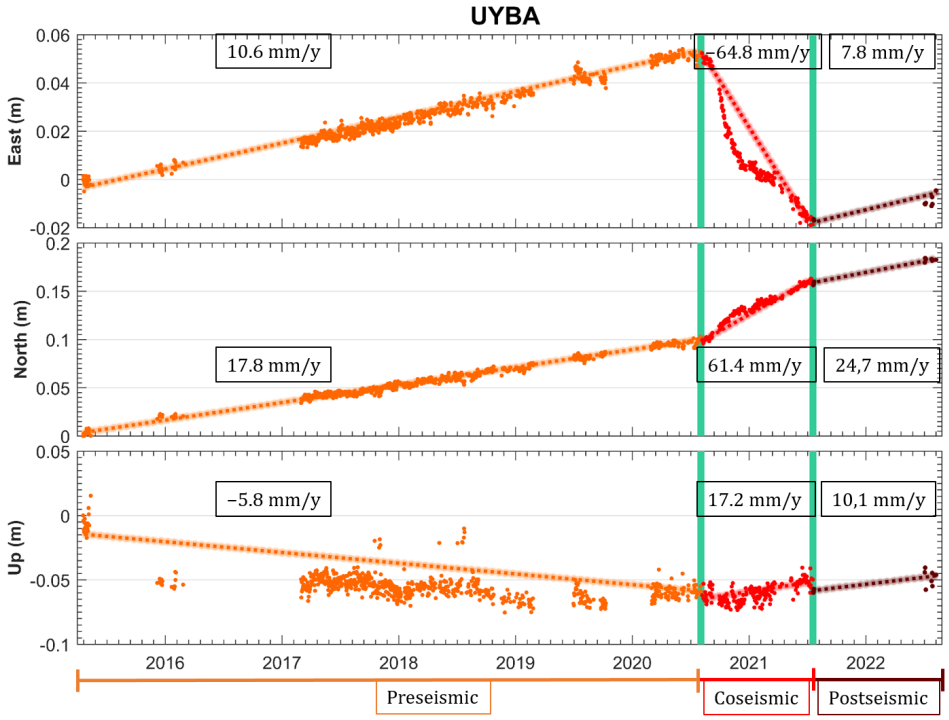

Figure 9. Topocentric time series of the UYBA station, separating the preseismic (orange), coseismic (red), and postseismic (brown) phases, and adding their linear fit. The corresponding velocities are shown in mm/year.

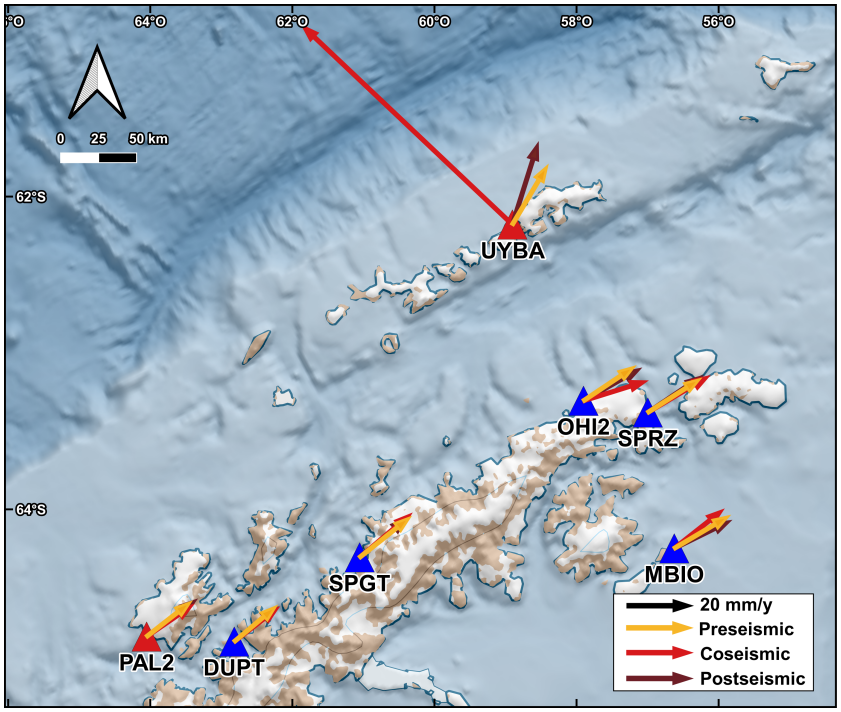

Figure 10. Preseismic, coseismic, and postseismic displacement model.

5. Conclusions

The region defined by the South Shetland Islands, the Bransfield Basin, and the Antarctic Peninsula is characterized by a highly complex tectonic environment. This region is also characterized by the presence of active volcanism, with emerged volcanoes, such as Deception, Penguin, and Bridgeman; and some underwater volcanic edifices, such as the Orca volcano. In 2020, intense seismic activity was recorded around the Orca volcano with earthquakes of up to 6.9 Mw.

This work focused on the analysis of the geodynamic activity that occurred in 2020 near the Orca volcano. The topocentric time series of the stations located in the region were analyzed: UYBA and PAL2, provided by the NGL. A descriptive analysis was carried out, adding the seismic events that occurred from 2015 to 2023. To estimate the trend in the series, two techniques were applied: a linear fit and MIDAS technique. The trend obtained from the linear fit was valid if the series presented a linear behavior (PAL2 time series). For nonlinear series (UYBA time series), the MIDAS estimator was applied. The displacement models of the region were obtained for each estimated velocity.

For a better understanding of the geodynamic process, the velocity of the preseismic, coseismic, and postseismic phases were estimated; the corresponding displacement models were obtained. These models showed that the preseismic and postseismic phases are similar in modulus and magnitude, while the coseismic phase presents different behavior.

Author Contributions: Conceptualization, B.R., M.B. and A.P.-P.; methodology, B.R., P.B., J.R.-Z. and M.B.; software, B.R. and P.B.; validation, M.B. and J.G.; formal analysis, B.R., J.R.-Z., V.J., J.G. and M.B.; investigation, B.R., V.J., R.M., E.C. and M.B.; resources, A.P.-P.; data curation, A.P.-P., A.d.G. and V.J.; writing—original draft preparation, B.R., M.B., A.P.-P., V.J., R.M. and E.C.; writing—review and editing, B.R and M.B.; visualization B.R. and J.R.-Z.; supervision, M.B. and J.G. All authors have read and agreed to the published version of the manuscript.

Funding: This research were possible thanks to the resources and funds of the astronomy, geodesy, and cartography laboratory of the University of Cadiz, directed by the principal researcher D. Manuel Berrocoso Domínguez.

Institutional Review Board Statement: Not applicable.

Informed Consent Statement: Not applicable.

Data Availability Statement: Data shown in this manuscript belong to the public catalog of the Nevada Geodetic Laboratory (NGL), http://geodesy.unr.edu/gps/ngl.acn.txt (accessed on 1 June 2023).

Acknowledgments: The contributions of both editor and of the reviewers are very much appreciated, which greatly helped to improve the manuscript.

Conflicts of Interest: The authors declare no conflict of interest.

References

1. Rosado, B.; Fernández-Ros, A.; Berrocoso, M.; Prates, G.; Gárate, J.; De Gil, A.; Geyer, A. Volcano-tectonic dynamics of Deception Island (Antarctica): 27 years of GPS observations (1991–2018). *J. Volcanol. Geotherm. Res.* **2019**, *381*, 57–82. [CrossRef]
2. Robertson-Maurice, S.D.; Wiens, D.A.; Shore, P.J.; Vera, E.; Dorman, L.M. Seismicity and tectonics of the South Shetland Islands and Bransfield Strait from a regional broadband seismograph deployment. *J. Geophys. Res.* **2003**, *108*, 2461. [CrossRef]
3. Ibáñez, J.M.; Carmona, E.; Almendros, J.; Saccorotti, G.; Del Pezzo, E.; Abril, M.; Ortiz, R. The 1998–1999 seismic series at Deception Island volcano, Antarctica. *J. Volcanol. Geotherm. Res.* **2003**, *128*, 65–88. [CrossRef]
4. Cesca, S.; Sugan, M.; Rudzinski, L.; Vajedian, S.; Niemz, P.; Plank, S.; Petersen, G.; Deng, Z.; Rivalta, E.; Vuan, A.; et al. Massive earthquake swarm driven by magmatic intrusion at the Bransfield Strait, Antarctica.*Commun. Earth Environ.* **2022**, *3*, 89. [CrossRef]
5. Olivet, J.L.; Bettucci, L.S.; Castro-Artola, O.A.; Castro, H.; Rodríguez, M.; Latorres, E. A seismic swarm at the Bransfield Rift, Antarctica. *J. S. Am. Earth Sci.* **2021**, *111*, 103412. [CrossRef]
6. Yuan, P.; Blewitt, G.; Kreemer, C.; Hammond, W.C.; Argus, D.; Yin, X.; Van Malderen, R.; Mayer, M.; Jiang, W.; Awange, J.; et al. An enhanced integrated water vapour dataset from more than 10000 global ground-based GPS stations in 2020. *Earth Syst. Sci. Data* **2023**, *15*, 723–743. [CrossRef]
7. Blewitt, G.; Hammond, W. C.; Kreemer, C. Harnessing the GPS data explosion for interdisciplinary science. *Eos* **2018**, *99*, 485. [CrossRef]
8. Bertiger, W.; Bar-Sever, Y.; Dorsey, A.; Haines, B.; Harvey, N.; Hemberger, D.; Heflin, M.; Lu, W.; Miller, M.; Moore, A.W.; et al. GipsyX/RTGx, a new tool set for space geodetic operations and research. *Adv. Space Res.* **2020**, *66*, 469–489. [CrossRef]
9. Zumberge, J.; Heflin, M.; Jefferson, D.; Watkins, M.; Webb, F. Precise point positioning for the efficient and robust analysis of GPS data from large networks. *J. Geophys. Res. Solid Earth* **1997**, *102*, 5005–5017. [CrossRef]
10. Barba, P.; Rosado, B.; Ramírez-Zelaya, J.; Berrocoso, M. Comparative Analysis of Sta-tistical and Analytical Techniques for the Study of GNSS Geodetic Time Series. *Eng. Proc.* **2021**, *5*, 21. [CrossRef]
11. Rosado, B.; Ramírez-Zelaya, J.; Barba, P.; De Gil, A.; Berrocoso, M. Comparative Analysis of Non-Linear GNSS Geodetic Time Series Filtering Techniques: El Hierro Volcanic Process (2010–2014). *Eng. Proc.* **2021**, *5*, 23.%2Fengproc2021005023. [CrossRef]
12. Blewitt, G.; Kreemer, C.; Hammond, W.C.; Gazeaux, J. MIDAS robust trend estimator for accurate GPS station velocities without step detection. *J. Geophys. Res. Solid Earth.* **2016**, *121*, 2054–2068. [CrossRef] [PubMed]
13. Reddy, C.D.; Arora, S.K.; Sunil, P.S.; Prajapati, S.K. Earthquake Related Deformation Cycle: Perspectives from 2004 Sumatra and 2010 Chile Mega-Earthquakes. *Disaster Adv.* **2011**, *4*, 13–21.